ACS Photonics

Article

pubs.acs.org/journal/apchd5

Coherent Coupling between a Molecular Vibration and Fabry−Perot Optical Cavity to Give Hybridized States in the Strong Coupling Limit

J. P. Long and B. S. Simpkins*

Chemistry Division, Naval Research Laboratory, 4555 Overlook Avenue SW, Washington, D.C. 20375, United States

Supporting Information

ABSTRACT: The coherent coupling between an optical transition and a confined optical mode, when sufficiently strong, gives rise to a new pair of mixed modes separated in frequency by the vacuum Rabi splitting. Such systems have been widely investigated for electronic-state transitions such as molecular excitons coupled to surface-plasmons and optical microcavities. However, only very recently have vibrational transitions been considered. Here we experimentally investigate the coupling between a Fabry−Perot cavity and the carbonyl stretch at an infrared frequency near 1730 cm^{-1} in polymethyl methacrylate. As is requisite for the "strong coupling" regime, the measured vacuum-Rabi-splitting of 132 cm^{-1} is much larger than the full width of either the cavity resonance (34 cm^{-1}) or the inhomogeneously broadened carbonyl-stretch absorption (24 cm^{-1}). With the assistance of quantitative analysis using transfer-matrix methods, we provide evidence that the mixed-state resonances are relatively immune to inhomogeneous vibrational broadening and demonstrate the ability to extract splittings by convenient angle tuning of the Fabry−Perot cavity to match the vibrational frequency. Opening the field of polaritonic coupling to vibrational species promises to be a rich arena amenable to a wide variety of infrared-active bonds that can be studied both statically (as here) and dynamically with ultrafast methods. Moreover, microfluidic cavities will permit the study of liquids, greatly expanding the range of assessable molecules.

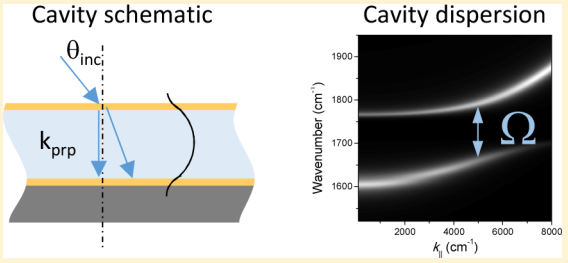

KEYWORDS: *vacuum Rabi splitting, strong coupling, infrared spectroscopy, optical cavity, vibrational coupling*

When an optical transition (e.g., a molecular excitonic absorption) is excited by a confined optical-mode oscillating at the same frequency (e.g., an optical microcavity), a strong coupling between the two resonances can occur. This coupled-oscillator system exhibits a hybridization of the two resonances to create two new eigenstates of mixed character that are each shifted from the original resonant frequency by half the vacuum Rabi splitting, Ω. Such coupled systems are variously referred to as cavity polaritons,[1] normal coupled modes,[2] more specific terms (e.g., plexitons[3]), or simply coupled-modes. These coupled-mode systems have received widespread attention in part because the split states possess new properties such as immunity to inhomogeneous broadening[4] or altered relaxation pathways.[5,6] The coupled systems can have marked implications for emission and relaxation rates and, accordingly, have found utility in the pursuit of nanoscale organic lasing materials[7] and nearly threshold-less lasers.[8,9] Cavities strongly coupled to single optical-emitters have also been considered for use in quantum information systems.[10−13]

To date, a wide variety of strategies spanning microwave to visible frequencies have been employed or proposed to produce the confined-mode, including surface-plasmon polaritons propagating on films[14,15] and on nanowires,[16] local surface plasmons,[17,18] Fabry−Perot cavities,[8] whispering gallery cavities,[11] photonic crystals,[10,19] and microwave cavities. The species coupled to the confined modes most commonly include electronic transitions such as the excitonic absorptions in molecules,[17,18,20] quantum wells,[2,13,21−23] and semiconducting[13] and colloidal quantum-dots,[24] as well as atomic transitions. Recently, the replacement of electronic transitions with microfabricated optomechanical oscillators operating at low temperature has also attracted intense scrutiny.[25]

Surprisingly, perhaps, there are very few reports utilizing modes in the infrared,[26,27] particularly vibrational modes.[26] Here we report coherent coupling between the carbonyl (-C═O) stretch in polymethyl methacrylate (PMMA) near 1730 cm^{-1} and the confined standing-wave mode of a Fabry−Perot (FP) cavity comprising a ∼2 μm thick spun-film of PMMA sandwiched between two Au mirrors 19 nm thick (Figure 1a). The coherent cycling of energy between these two states reaches the so-called strong-coupling regime, which is attained when the coupling strength between the vibrational and cavity modes exceeds the average of their decay rates, as evidenced by our measured vacuum Rabi splitting (Ω ∼ 132 cm^{-1}) being much larger than the full-width-at-half-maximum (fwhm) of either the cavity (∼34 cm^{-1}) or inhomogeneously broadened carbonyl absorption (24 cm^{-1}). Normal-mode coupling involving vibrational absorptions offers an attractive experimental system amenable to a wide variety of molecular vibrations. It is possible that the coherently excited population of vibrations may generate a macroscopic mechanical response.

Received: September 9, 2014
Published: November 14, 2014

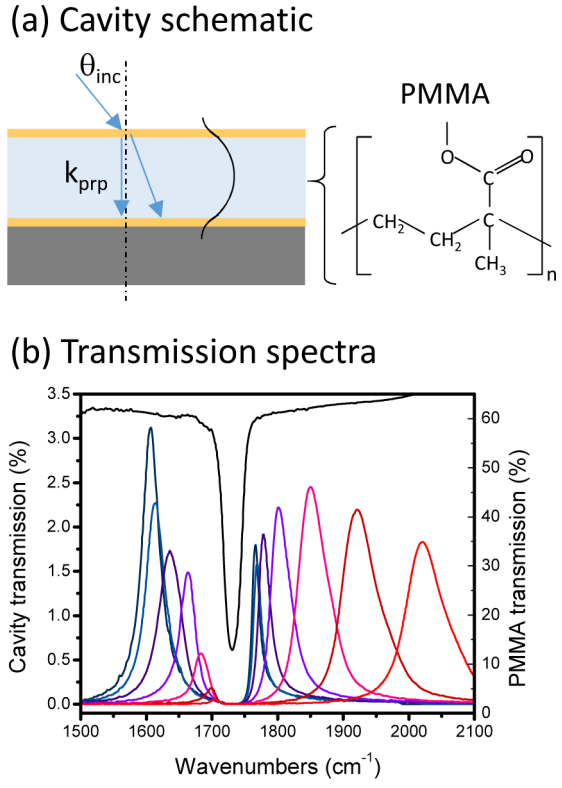

Figure 1. (a) Cross section of the Au/PMMA/Au Fabry–Perot cavity on a silicon substrate, with schematics of the incident and refracted rays, the m = 1 half-wave resonance field-intensity, and the PMMA monomeric unit. (b) FTIR transmission spectrum of bare PMMA film (black curve with negative going valley) and a subset of the transmission spectra of the full cavity for angles of incidence θ_{inc} from 0° to 60° in steps of 10° from left to right.

We anticipate that the large wavelengths involved (~3–17 μm, accounting for a typical intracavity refractive index of 1.3) should enable the construction of microfluidic etalons for examining liquids, especially when higher-order FP modes are exploited to increase the spacing between mirrors. We also expect ultrafast vibrational methods[28,29] to offer additional insights into coupled-state dynamics analogous to studies in coupled electronic systems.[5,6]

Cavities coupled to a two-level absorber are describable with a quantized photon field for any number of absorbers down to a single one. However, for our case, where a large number of carbonyl bonds are involved, a purely classical treatment that employs transfer-matrix methods[22] or the relatively simple expression for the transmission through a FP cavity[2,21,30] are applicable. We also note that, in this regime (i.e., where many oscillators are available), the system does not behave in the markedly quantum-mechanical manner exhibited when a single cavity-coupled atom responds to a single photon by, for example, blocking transmission through the cavity, or to two photons by climbing the Jaynes-Cummings ladder.[2,13] To distinguish this highly nonlinear quantum-dominated regime, the term "true strong-coupling" is sometimes applied, as detailed in ref 13. Here we adopt the nomenclature employed by the extensive literature on cavity-coupling to macroscopic electronic-systems that refer to avoided crossings as the strong-coupling regime.[7,3,22,31,32]

We exploit the classical behavior of macroscopic systems to design FP cavities that can be angle-tuned through the carbonyl absorption band to match the resonant condition and to provide a comprehensive analysis of the resulting transmission measurements. Unlike the alternative approach of adjusting the FP-cavity thickness to match the vibrational frequency,[26] angle-tuning only one cavity is experimentally more expedient, while also ensuring the correct measurement of the vacuum Rabi splitting as the smallest splitting between the hybridized modes as angle is tuned. We verify that the classical predictions compare well to the measured dispersion of the coupled states, and to the inferred vacuum Rabi splitting. We also confirm the utility of employing either s- or p-polarized excitation, opening the way to probe materials that might possess differing in- and out-of-plane molecular orientations or environments. Finally, we demonstrate an insensitivity of the hybridized-mode line widths to the significant inhomogeneous broadening of the carbonyl resonance, as theoretically expected, and which offers the prospect of measuring homogeneous vibrational line widths directly if the "empty cavity" resonant width is known.

METHODS

As illustrated in Figure 1a, samples consist of a planar Au/PMMA/Au Fabry–Perot cavity fabricated via e-beam evaporation of Au mirrors and spinning of PMMA (molecular weight 950 kDa) on an undoped silicon wafer coated with a 3 nm Cr adhesion layer. The metal thicknesses were based on calibrated evaporation rates, while the PMMA thickness was measured with a stylus profilometer on a witness film spun under conditions identical to the cavity film. Target values were 20 nm for Au and 2120 nm for the PMMA. The PMMA thickness was chosen so that the cavity resonant frequency would sweep through the carbonyl absorption at an angle of incidence of ~30°. Based on transfer-matrix modeling of the measured reflectance from a gold witness film and the measured cavity-dispersion with angle, the Au and PMMA thicknesses used for analysis were adjusted to 19 and 2054 nm, well within the uncertainty of the target thicknesses.

Angle- and polarization-dependent transmittance spectra were obtained in a Fourier-transform infrared (FTIR) spectrometer (Thermo Scientific) equipped with a wire-grid polarizer and a home-built sample rotator. Data were taken with 4 cm^{-1} resolution, which contributed negligibly ($\leq$0.5 cm^{-1}) to the measured absorption line widths discussed below. A single background for each polarization was used for transmission. We operated the FP cavity in first order (the half-wave resonance) and tuned its resonant wavelength by adjusting the angle of incidence. Bare PMMA on Si was characterized with FTIR transmission spectroscopy. Reflection FTIR spectroscopy characterized the reflectance of a Au witness film deposited on Si during the same evaporation as cavity production.

Numerical modeling of the system transmission and reflectance was accomplished via the transfer matrix approach within the WVASE software package.[33] The set of ellipsometrically determined optical-constants (n and k) for PMMA provided by the software accurately predicted the measured frequency at minimum transmission for the carbonyl band in a bare PMMA film (1731 cm^{-1} experiment; 1732 cm^{-1} via n and k). The transmission spectrum predicted by the optical constants similarly agreed with the width of the measured transmission band (29 cm^{-1}) to within a wavenumber, and also predicted a ~Gaussian line shape, as measured.

dx.doi.org/10.1021/ph5003347 | ACS Photonics 2015, 2, 130–136

RESULTS AND DISCUSSION

Mode Dispersion. Shown in Figure 1b are representative transmission spectra taken of the full cavity structure at various angles as well as a spectrum of the bare PMMA film on undoped Si (no Au mirrors). The bare transmission spectrum shows the C═O stretch to be centered at ∼1731 cm^{-1} and to have a measured Gaussian fwhm of ∼24 cm^{-1}. The presence of two peaks in the full-cavity transmission illustrates the modal splitting due to coupling between the optical cavity and the C═O vibrational stretch. The modal splitting leaves a void in the spectral response where the uncoupled vibrational band resides.

Angle-dependent spectra, as in Figure 1b, can be assembled into intensity-contour plots representing the full dispersion of the coupled cavity-vibration system, as shown in Figure 2a,b,

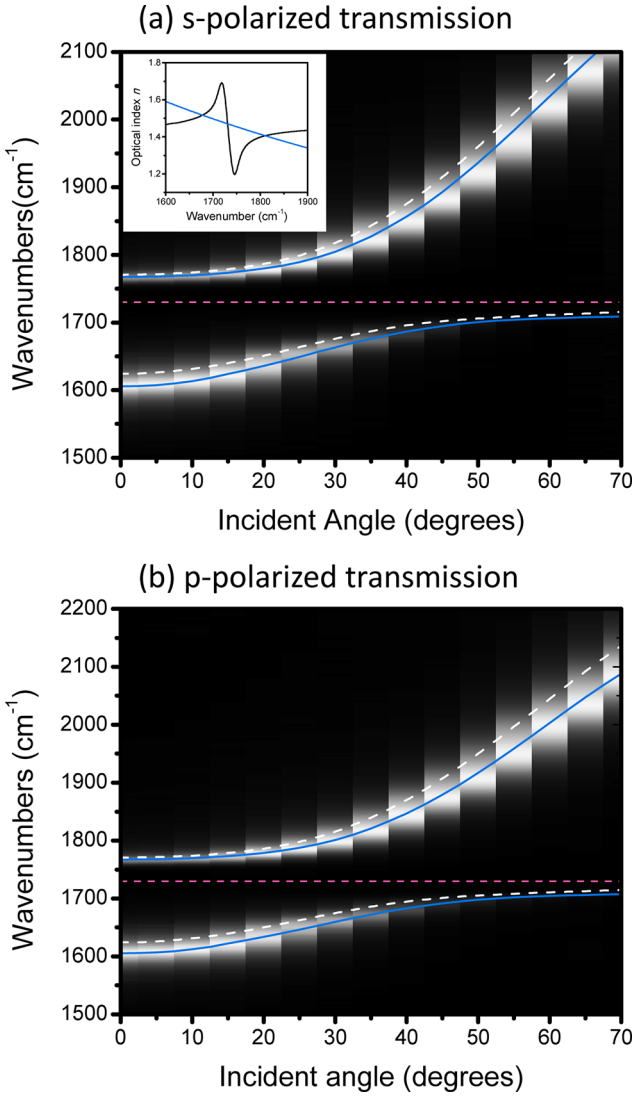

Figure 2. (a) Experimental angular-dispersion of transmission spectra displayed as an intensitycontour plot for s-polarized excitation. Horizontal dashed line marks the bare PMMA absorption. Blue and white curves give the dispersion computed, respectively, with transfer-matrix methods and the resonance condition for a Fabry−Perot cavity. Inset: refractive index of PMMA (black curve) and right-hand side of eq 2 (blue curve). Graphical solution to the coupled-mode resonance condition is found at the crossing points. (b) Same as (a) for p-polarized incident radiation.

for incident s- and p-polarizations. Here, transmission spectra were recorded as the angle of incidence was stepped every 5°. The position of the uncoupled C═O stretch mode, which occurs at a frequency $\overline{\nu_0} \sim 1731$ cm^{-1}, is indicated by the horizontal dashed line. Coupling between the optical cavity mode and the vibrational mode is seen as an avoided crossing of two branches. At 0°, the upper branch (UB) near 1760 cm^{-1} is primarily of vibrational character, and the lower branch (LB) near 1600 cm^{-1} is mainly of cavity character. As the incident angle is increased, the lower branch tunes through the bare vibrational absorption frequency, but mode hybridization leads to an avoided crossing when the cavity becomes resonant with the C═O absorption, near 30° as designed. By 50°, the character of the two branches has switched, and the UB disperses rapidly with angle in accord with FP-cavity behavior. The displacement from the bare C═O stretch of the LB at 0° and the UB at 70° indicates some degree of coupling, even under these nonresonant conditions.

In Figure 2a,b, it is evident that the dispersion and branch splittings are very similar for s- and p-polarized excitation. The slightly weaker dispersion for p-polarized incidence in the UB at the largest incidence angles is due simply to the larger phase shift φ upon reflection of p-polarized waves internal to the cavity (see eqs 1 and 2 below). For incident angles where the two branches most closely approach vertically (the approximate vacuum Rabi splitting), s- and p-incidence give nearly identical results. We emphasize that p-polarization excites both in- and out-of-plane vibrations, while s-polarized conditions produce only in-plane motion. This may have implications for the direction of the resulting mechanical work and modulation of the cavity's optical response if one can control the orientation of the vibrational modes of interest. Furthermore, s- and p-polarized excitation of the cavity produce different field distributions: s-polarized excitation yields a field maximum at the cavity's center, while p-polarization yields both in-plane and normal field components with the normal component peaked at the mirrors (see Supporting Information). Thus, polarization control may allow one to selectively couple to either in-plane or out-of-plane oriented dipole-ensembles and constrain the spatial region within the cavity that is most strongly coupled.

Superposed on Figure 2a,b are curves derived from classical optical considerations. The solid blue curves, obtained with transfer-matrix algorithms in the WVASE software package, give excellent agreement over the entire range. The dashed white curves give the resonance condition derived from the transmission function $T(\overline{\nu})$ for a planar FP cavity containing an absorptive medium:[2,21,30]

$$T(\overline{\nu}) = \frac{|t_1 t_2| e^{-\alpha L}}{1 + |r_1 r_2|^2 e^{-2\alpha L} - 2|r_1 r_2| e^{-\alpha L} \cos(4\pi n L \cos(\theta)\overline{\nu} + \varphi_1 + \varphi_2)} \quad (1)$$

where t_i and r_i, are, respectively, the transmission and reflectance amplitudes at mirror i, L is the cavity thickness, α is the absorption coefficient, n is the index of refraction, and θ is the angle of an incident ray after refraction within the PMMA. The reflection phase-shifts at each mirror, ϕ_i, account for the cavity mode penetration into the Au mirrors. All quantities except L are frequency-dependent. By inspection, if r_i, t_i, and α are slowly varying, $T(\overline{\nu})$ peaks near a resonant frequency $\overline{\nu}_r$, where the cosine term is zero. This occurs when the argument of the cosine equals $2\pi m$, where m is the mode order, which can be arranged to give the FP resonance condition:

dx.doi.org/10.1021/ph5003347 | ACS Photonics 2015, 2, 130−136

$$n(\bar{\nu}_r) = [2\pi m - \varphi_1(\bar{\nu}_r) - \varphi_2(\bar{\nu}_r)]/4\pi L \cos(\theta)\bar{\nu}_r \quad (2)$$

To produce the white dashed curves in Figure 2a,b, eq 2 was solved numerically at each angle of incidence. However, that there are multiple branches can be readily seen from a graphical solution, as illustrated in the inset to Figure 2a, where the left and right sides of eq 2 are plotted versus $\bar{\nu}$ at fixed internal angle of ~17°, near the angle of maximum coupling. It can be seen that there are three roots, but the center root produces an almost negligible transmission peak because of strong absorption. To carry out the numerical solution to eq 2, the (real) PMMA refractive index $n(\bar{\nu})$ (inset to Figure 2a) was obtained from the WVASE software package.[33] This refractive index was also used in Snell's law to compute the internal propagation angle, θ, and in formulas[30] for the phase shifts upon reflection from the thin Au mirrors. However, we did not apply involved corrections to Snell's law or to the reflectance phase for an absorptive medium.[34,35] While the dispersion given by eq 2 agrees with the measured dispersions in Figure 2a,b less well than does the transfer matrix approach, it is nevertheless quite satisfactory for designing cavities prior to fabrication and indicates that one may quickly predict the approximate vacuum Rabi splitting for a wide range of material excitations, given the frequency-dependent refractive index of the material.

In Figure 3a, we display the frequency difference between the LB and UB for our s-polarized experimental results (symbols) and for the transfer-matrix simulations (solid curve) that gave the blue dispersion curves of Figure 2. Similarly, in Figure 3b, we compare the experimental FWHMs of the two branches to the FWHMs of the simulation after accounting for instrumental broadening as described below. The strong agreement between the computations and the experiment for both the dispersion and the widths lends confidence that the simulations may be used for further analysis.

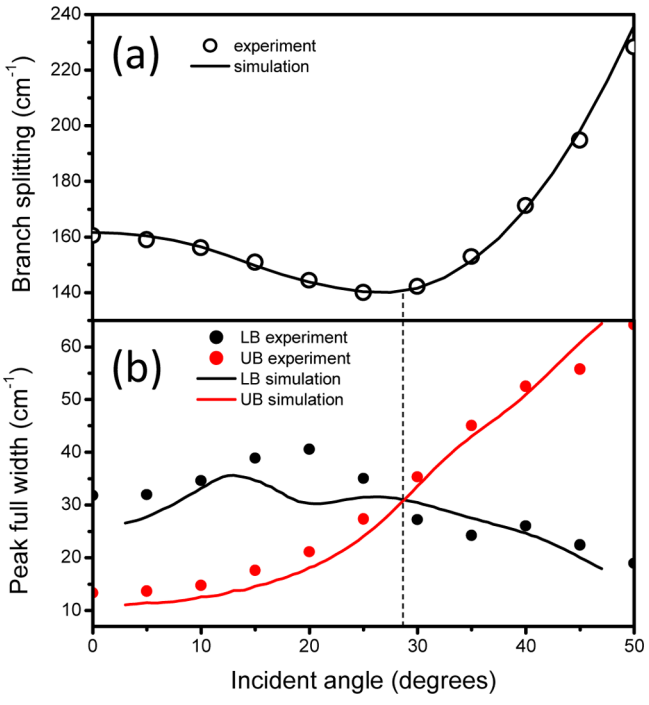

Figure 3. (a) Measured dependence on incident angle of the vertical splitting between the coupled-mode upper and lower branches of Figure 2a for s-polarized excitation (symbols) and splitting predicted by transfer-matrix methods (curve). (b) Measured spectral FWHMs of the branches (symbols) and transfer matrix computations (solid curves) after broadening to account for the 6° full angular spread of the FTIR beam. Vertical line is guide to the eye.

The measured minimal splitting in Figure 3a has a value Ω = 140 cm^{-1}; the results for p-polarized excitation give an almost identical splitting of 141 cm^{-1} (see Supporting Information). While this smallest value for the energy separation is nearly equal to the vacuum Rabi splitting, it must be corrected for (i) having been measured in a transmission experiment,[22] as discussed below, and (ii) for having been derived from an off-normal measurement, where the cavity was angle-tuned to the absorber frequency. In this case, one must be mindful that the two hybridized modes assume different internal wavevectors for any particular angle of incidence, a consequence of the strong frequency dependence of the refractive index (inset to Figure 2a). To reflect the coherence giving rise to the hybridization, angular-dispersion curves such as displayed in Figure 2 can be replotted versus the in-plane component of the wavevector.[1] The in-plane component is the same both inside and outside the PMMA cavity, and is given by $k_{||} = k_0 \sin(\theta)$, where θ is the angle of incidence and k_0 is the free space wavevector $2\pi\bar{\nu}$. (For each of the hybridized modes on-resonance, the perpendicular component is automatically matched by the geometrical half-wave resonance condition of the FP cavity.)

Instead of plotting the experimental data of Figure 2 versus $k_{||}$, it is more informative to use the higher point density available from the transfer-matrix simulation, which accurately represent experiment (see agreement in Figures 2 and 3). Figure 4a shows the resulting $k_{||}$ dispersion, and Figure 4b shows the vertical splitting between upper and lower branches. Here the minimum splitting is Ω_T = 132 cm^{-1} ≈ Ω, measurably smaller than the vertical splitting of 140 cm^{-1} found in an angular dispersion plot (Figures 2 and 3a). This splitting of 132 cm^{-1} is consistent with theoretical predictions, as we discuss below after estimating quantities needed by the theory, namely, the homogeneous absorption line width Γ_H, the cavity line width, and the central absorption coefficient α_0. Similar analysis applied to data acquired with p-polarized incident light also finds Ω_T = 132 cm^{-1}, the same value as for s-polarized (see Supporting Information).

Rather than angle tuning the cavity, one may instead excite at normal incidence and vary the cavity thickness to match its resonance frequency to the absorber frequency.[26] This approach is less convenient, requiring multiple fabrications to find the minimum splitting, but it automatically achieves phase matching between the hybridized modes on-resonance. The inset to Figure 4b displays the splitting computed with the transfer-matrix code for normal incidence as cavity thickness is varied, reaching a minimum value of 132 cm^{-1}, in agreement with the splitting of 132 cm^{-1} derived from the angle-tuned simulation when plotted versus $k_{||}$. It is interesting to note that this vacuum Rabi splitting for the carbonyl stretch in PMMA is considerably less than the value of 167 cm^{-1} reported by Ebbeson et al. measured at normal incidence for the same bond in another ester-based material, polyvinyl acetate.

Resonance Widths. Figure 3b plots the measured fwhm of the upper and lower branches excited with s-polarized radiation. The two branch-widths vary with angle but assume very similar values near the angle of minimal branch splitting (i.e., where the carbonyl and cavity are fully coupled). To compare to transfer-matrix computations, we must account for instrumental broadening due to an angular spread in the weakly focused

dx.doi.org/10.1021/ph5003347 | ACS Photonics 2015, 2, 130−136

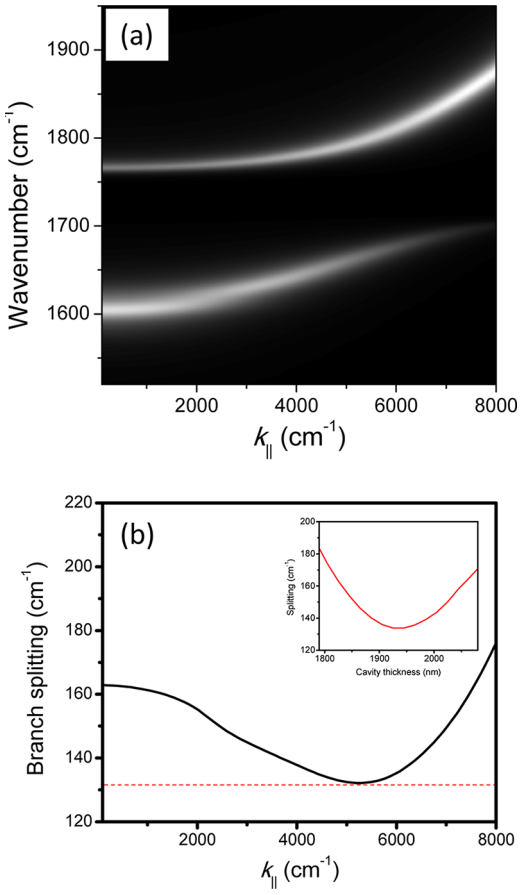

Figure 4. (a) Cavity dispersion plotted vs in-plane wavevector. (b) Vertical splitting between branches in (a), giving a Rabi vacuum splitting of 132 cm^{-1}. Inset: dispersion of the branch splitting with cavity thickness.

FTIR beam interrogating the sample, which we measured with a scanned knife-edge to be ~6° (full angle). The solid curves in Figure 3b plot the fwhm derived from computations that have been broadened by the 6° spread. The agreement is quite good; in particular, near the incident angle giving a minimum splitting between branches at 27.5°, the broadened transfer-matrix simulations of the two branch widths average to 29.9 cm^{-1}, very near the measured line width of ~31.2 cm^{-1}. (For p-polarized measurements and computations, the branch widths are, respectively, 32.6 and 29.9 cm^{-1}.)

To compare the measured widths to the theoretical expectation for coupled modes, we must first transform angular-dispersion results to $k_{||}$-dispersion as we did earlier to find the proper splitting between branches. To this end, we again employ the finer resolution available from the computations of Figure 4a. The average width of the two branches in Figure 4a at the value of $k_{||}$, where the branch splitting is minimum is found to be 21.4 cm^{-1}. This is to be compared to the theoretical width for the coupled modes, given as[4]

$$\Gamma_{CM} = (\Gamma_H + \Gamma_{cav})/2 \quad (3)$$

which requires that we estimate Γ_H, the homogeneous width of the interacting absorbent species (the carbonyl stretch), and Γ_{cav}, the width of the "empty cavity" resonance, that is, the width of the FP cavity unperturbed by the presence of the absorbent species.[21] These widths are also of interest because they appear in standard predictions for the vacuum Rabi splitting Ω, and in and corrections to Ω when measured in transmission treated below.[22] More importantly, because we find the carbonyl absorption to exhibit a clear Gaussian line shape, indicative of significant inhomogeneous broadening, the widths of the hybridized modes are of interest to affirm the prediction of their relative immunity to inhomogeneity.[4,23]

The homogeneous vibrational width Γ_H in eq 3 is not directly available because the absorptivity $\alpha_{expt}(\bar{\nu})$ derived from the transmission through a 2 μm PMMA film spun on Si, Figure 1b, displays a nearly Gaussian line shape for the carbonyl band with FHWM Γ_{CO} = 23.6 cm^{-1}, rather than the Lorentzian line shape of a homogeneously broadened absorber. Similarly, a Gaussian line shape with fwhm of 24.0 cm^{-1} is found for the absorptivity $\alpha_k(\bar{\nu})$ obtained from the ellipsometrically determined extinction coefficient $k(\bar{\nu})$ of PMMA.[33] To estimate Γ_H, we fit these two absorptivities with a "Voigt" function[36] generated by numerically broadening a Lorentzian-based homogeneous model-absorptivity with a Gaussian distribution of resonant frequencies (see Supporting Information). The resultant Lorentzian contribution, 2 cm^{-1}, is too small to materially affect the nonlinear least-squares fit, but indicates a homogeneous contribution much less than the overall fwhm of ~24 cm^{-1}. To set bounds on Γ_H, we inspected Voigt lineshapes fitted to $\alpha_{expt}(\bar{\nu})$ and $\alpha_k(\bar{\nu})$, while fixing Γ_H to increasingly large values, and based on the deterioration of the fit, place an upper limit on Γ_H of 5−10 cm^{-1}. These values are consistent with Lorentzian widths measured for the carbonyl band in PMMA by near-field scattering.[37]

We also cannot measure the empty-cavity width Γ_{cav} directly, because it is not possible to remove the carbonyl moiety from PMMA. However, an estimate can be obtained from the width of the second-order cavity resonance (m = 2; ν_2 ~ 3180 cm^{-1}) where perturbations due to vibrational absorptions are insignificant. The second-order transmission line shape conformed very accurately to a Lorentzian line shape (fwhm Γ_2 ~ 52 cm^{-1}; Gaussian contribution only ~11 cm^{-1} fwhm via fitting a Voigt function). This is consistent with eq 1, which predicts a Lorentzian shape for the resonance spectrum when the mirror reflectances are high, with a width proportional to $(1 - |r_1 r_2|^2)/|r_1 r_2|$.[22,30] The width Γ_{cav} of the first-order cavity mode will be smaller because the Au optical conductivity and, hence, the r_i, is larger at lower frequency. After making this correction using optical constants for Au,[33] we estimate Γ_{cav} ~ 34 cm^{-1}. Further details are found in the Supporting Information.

Using the above estimates (Γ_{cav} = 34 cm^{-1} and $\Gamma_H \leq 10$ cm^{-1}), eq 3 predicts branch line widths on resonance to be Γ_{CM} = 22 cm^{-1} or less. This is entirely consistent with the average of the branch widths, 21.4 cm^{-1}, computed with the transfer-matrix code as noted above. Hence, present data, pertinent to the relatively new regime of cavity/vibrational-mode coupling, support the expectation that strong coupling yields hybridized modes that are relatively immune to the inhomogeneous broadening that is universally encountered in solid materials.

Comparison of Rabi Splitting to Analytical Approximation. With the widths of the unperturbed cavity and vibrational mode known, one may predict the vacuum Rabi splitting, Ω, the key parameter describing the coupling strength between the cavity and the carbonyl stretching mode. Standard expressions approximating Ω,[2,21] when expressed in wavenumbers, give

dx.doi.org/10.1021/ph5003347 | ACS Photonics 2015, 2, 130−136

$$\Omega = \sqrt{\frac{\alpha_0 \Gamma_H}{2\pi n_B} - \frac{(\Gamma_H - \Gamma_{cav})^2}{2}} \quad (4)$$

where α_0 is the maximal absorbance of the active species (here, the carbonyl stretch) and n_B is the "background" refractive index. Savona et al., have emphasized that a transmission experiment measures a slightly different splitting given by

$$\Omega_T = \sqrt{\sqrt{\left(\frac{\alpha_0 \Gamma_H}{2\pi n_B}\right)^2 + \frac{\alpha_0 \Gamma_H}{\pi n_B}\Gamma_H(\Gamma_H + \Gamma_{cav})} - {\Gamma_H}^2} \quad (5)$$

For systems as strongly coupled as ours, the splitting is strongly dominated by the first term on the right-hand side of eqs 4 and 5; substituting the widths derived in the previous section finds that the other terms affect both splittings by less than 1 cm^{-1}. However, the first term is sensitive to the value of Γ_H and to the value of α_0 that corresponds to this *homogeneous* width. An estimate of α_0 is provided automatically when one estimates Γ_H by fitting $\alpha_k(\bar{\nu})$ or $\alpha_{expt}(\bar{\nu})$ with the well-accepted model-function for a homogeneously broadened absorption,[38] as carried out in the previous section and detailed in Supporting Information. For homogeneous widths $5 < \Gamma_H < 10$ cm^{-1}, we find the corresponding central absorptivity is bounded as $5 \times 10^4 > \alpha_0 > 2.7 \times 10^4$ cm^{-1} when fitting the absorptivity $\alpha_k(\bar{\nu})$, the peak value of which we deem to be quantitatively more reliable than our FTIR determination. The corresponding theoretical range for the Rabi splitting from eq 4 is $122 < \Omega < 132$ cm^{-1}. The corresponding range for the splitting in a transmission experiment predicted by eq 5 is barely larger, $123 < \Omega_T < 132$ cm^{-1}, showing that the splitting of 132 cm^{-1} determined from our transmission experiments reliably estimates the Rabi splitting.

Equation 4 or 5 provides a useful guide for selecting molecular vibrations to target in cavity-coupling studies. One generally has some knowledge of the absorptivity and width of the vibration of interest through standard absorbance measurements, which allows estimating the first term under the radicals. If this term is much greater than the expected widths of the cavity and vibrational modes, the strong coupling regime should pertain. Otherwise, weak coupling is expected, which can lead to an interference between the cavity and the absorptive mode, giving rise to a Fano line shape.[39] Similar weak coupling can be expected for weaker vibrations near the target absorption, a situation we intentionally avoided to simplify the analysis of these data.

CONCLUSION

We have brought strong polaritonic coupling from the visible regime, where coupling to electronic transitions have been investigated for two decades, into the infrared where a new range of static and dynamic vibrational processes await investigation. Strong polaritonic coupling between an optical cavity and a carbonyl vibrational-transition was demonstrated using an angle-tuned Fabry−Perot microcavity. We have shown how to correct for phase-mismatch in an angle-tuned experiment and, once applied, determined a vacuum Rabi splitting of 132 cm^{-1}. This splitting is ∼4× larger than the cavity mode width and >5× the unperturbed vibrational mode width qualifying this response as strong coupling. This response is in excellent agreement with transfer-matrix predictions and with standard analytical expressions approximating the Rabi splitting. Further quantitative analysis finds that the widths of the hybridized modes are relatively unaffected by inhomogeneous broadening, in accord with theoretical expectations. Extending the strong polaritonic-coupling, long known for electronic transitions to infrared vibrational states, should open a range of new possibilities, including a wide array of molecular vibrations; static as well as ultrafast studies of the dynamics of strongly coupled systems under various degrees of inhomogeneous broadening; and research venues greatly expanded from solids to liquids.

ASSOCIATED CONTENT

Supporting Information

Additional experimental details and figures. This material is available free of charge via the Internet at http://pubs.acs.org.

AUTHOR INFORMATION

Corresponding Author

*E-mail: blake.simpkins@nrl.navy.mil.

Notes

The authors declare no competing financial interest.

ACKNOWLEDGMENTS

Research was funded by the Office of Naval Research Nanoscience Institute Program 61-P087-13. The authors thank Dr. J. C. Owrutsky and Dr. Igor Vurgaftman for enlightening discussion and guidance and Erik Johnson for measuring the angular spread of the FTIR beam.

REFERENCES

(1) Agranovich, V. M.; Litinskaia, M.; LIdzey, D. G. Cavity polaritons in microcavities containing disordered organic semiconductors. *Phys. Rev. B* **2003**, *67*, 085311.

(2) Khitrova, G.; Gibbs, H. M.; Jahnke, F.; Kira, M.; Koch, S. W. Nonlinear optics of normal-mode-coupling semiconductor microcavities. *Rev. Mod. Phys.* **1999**, *71*, 1591−1639.

(3) Fofang, N. T.; Grady, N. K.; Fan, Z.; Govorov, A. O.; Halas, N. J. Plexciton dynamics: Exciton plasmon coupling in a J-aggregate−Au nanoshell complex provides a mechanism for nonlinearity. *Nano Lett.* **2011**, *11*, 1156−1560.

(4) Houdré, R.; Stanley, R. P.; Ilegems, M. Vacuum-field Rabi splitting in the presence of inhomogeneous broadening: Resolution of a homogeneous linewidth in an inhomogeneously broadened system. *Phys. Rev. A* **1996**, *53*, 2711−2715.

(5) Gomez, D.; Lo, S. S.; Davis, T. J.; Hartland, G. V. Picosecond kinetics of strongly coupled excitons and surface plasmon polaritons. *J. Phys. Chem. B* **2013**, *117*, 4340−4346.

(6) Norris, T. B.; Rhee, J.-K.; Sung, C.-Y.; Arakawa, Y.; Nishioka, M.; Weisbuch, C. Time-resolved vacuum Rabi oscillations in a semiconductor quantum microcavity. *Phys. Rev. B* **1994**, *50*, 14663−14666.

(7) Tischler, J. R.; Bradley, M. S.; Zhang, Q.; Atay, T.; Nurmikko, A.; Bulović, V. Solid state cavity QED: Strong coupling in organic thin films. *Org. Electron.* **2007**, *8*, 94−113.

(8) Yokohama, H. Physics and device applications of optical microcavities. *Science* **1992**, *256*, 66.

(9) Yokoyama, H.; Suzuki, M.; Nambu, Y. Spontaneous emission and laser oscillation properties of microcavities containing a dye solution. *Appl. Phys. Lett.* **1991**, *58*, 2598.

(10) Englund, D.; Shields, B.; Rivoire, K.; Hatami, F.; Vučković, J.; Park, H.; Lukin, M. D. Deterministic coupling of a single nitrogen vacancy center to a photonic crystal cavity. *Nano Lett.* **2010**, *10*, 3922−3926.

(11) Park, Y.-S.; Cook, A. K.; Wang, H. Cavity QED with diamond nanocrystals and silica microspheres. *Nano Lett.* **2006**, *6*, 2075−2079.

(12) Kasprzak, J.; Richard, M.; Kundermann, S.; Baas, A.; Jeambrun, P.; Keeling, J. M. J.; Marchetti, F. M.; Szymańska, M. H.; André, R.; Staehli, J. L.; Savona, V.; Littlewood, P. B.; Deveaud, B.; Dang, L. S.

Bose−Einstein condensation of exciton polaritons. *Nature* **2006**, *443*, 409−414.
(13) Khitrova, G.; Gibbs, H. M.; Kira, M.; Koch, S. W.; Scherer, A. Vacuum Rabi splitting in semiconductors. *Nat. Phys.* **2006**, *2*, 81−90.
(14) Pockrand, I.; Swalen, J. D.; Gordon, J. G.; Philpott, M. R. Exciton−surface plasmon interactions. *J. Chem. Phys.* **1979**, *70*, 3401−8.
(15) Pockrand, I.; A; Brillante, A.; Möbius, D. Exciton−surface plasmon coupling: An experimental investigation. *J. Chem. Phys.* **1982**, *77*, 6289−95.
(16) Liang, H.; Ruan, S.; Zhang, M.; Su, H.; Li, I. L. Modified surface plasmon polaritons for the nanoconcentration and long-range propagation of optical energy. *Sci. Rep.* **2014**, *4*, 1−4.
(17) Ambjornsson, T.; Mukhopadhyay, G.; Apell, S. P.; Kall, M. Resonant coupling between localized plasmons and anisotropic molecular coatings in ellipsoidal metal nanoparticles. *Phys. Rev. B* **2006**, *73*, 085412.
(18) Fofang, N. T.; Grady, N. K.; Fan, Z.; Govorov, A. O.; Halas, N. J. Plexciton dynamics: Exciton−plasmon coupling in a J-aggregate−Au nanoshell complex provides a mechanism for nonlinearity. *Nano Lett.* **2011**, *11*, 1556−60.
(19) Yoshie, T.; Scherer, A.; Hendrickson, J.; Khitrova, G.; Gibbs, H. M.; Rupper, G.; Ell, C.; Shchekin, O. B.; Deppe, D. G. Vacuum Rabi splitting with a single quantum dot in a photonic crystal nanocavity. *Nature* **2004**, *432*, 200−203.
(20) Canaguier-Durand, A.; Devaux, E.; George, J.; Pang, Y.; Hutchison, J. A.; Schwartz, T.; Genet, C.; Wilhelms, N.; Lehn, J.-M.; Ebbesen, T. W. Thermodynamics of molecules strongly coupled to the vacuum field. *Angew. Chem., Int. Ed.* **2013**, *52*, 10533−10536.
(21) Zhu, Y.; Gauthier, D. J.; Morin, S. E.; Wu, Q.; Carmichael, H. J.; Mossberg, T. W. Vacuum Rabi splitting as a feature of linear-dispersion theory: Analysis and experimental observations. *Phys. Rev. Lett.* **1990**, *64*, 2499.
(22) Savona, V.; Andreani, L. C.; Schwendimann, P.; Quattropani, A. Quantum well excitons in semiconductor microcavities: Unified treatment of weak and strong coupling regimes. *Solid State Commun.* **1995**, *93*, 733−739.
(23) Ell, C.; Prineas, J.; Nelson, T. R.; Park, S.; Gibbs, H. M.; Khitrova, G.; Koch, S. W.; Houdré, R. Influence of structural disorder and light coupling on the excitonic response of semiconductor microcavities. *Phys. Rev. Lett.* **1998**, *80*, 4795−4798.
(24) Le Thomas, N.; Woggon, U.; Schöps, O.; Artemyev, M. V.; Kazes, M.; Banin, U. Cavity QED with semiconductor nanocrystals. *Nano Lett.* **2006**, *6*, 557−561.
(25) Aspelmeyer, M., Kippenberg, T. J., Marquardt, F., Eds. *Cavity Optomechanics: Nano- and Micromechanical Resonators Interacting with Light*; Springer-Verlag: Berlin, Heidelberg, 2014.
(26) Shalabney, A.; George, J.; Hutchison J. A.; Pupillo,, G.; Genet, C.; Ebbesen, T. W. Coherent coupling of molecular resonators with a micro-cavity mode. *arXiv:1403.1050v1* **2014**, [quant-ph].
(27) Esteban, R.; Aizpurua, J.; Bryant, G. W. Strong coupling of single emitters interacting with phononic infrared antennae. *New J. Phys.* **2014**, *16*, 013052.
(28) Owrutsky, J. C.; Raftery, D.; Hochstrasser, R. M. Vibrational relaxation dynamics in solutions. *Annu. Rev. Phys. Chem.* **1994**, *45*, 519−555.
(29) Xu, Q.; Fayer, M. D. Vibrational dynamics of a metalloporphyrin carbonyl in liquid and glass solutions: ultrafast 1-D and frequency-selected vibrational echo experiments. *Laser Phys.* **2002**, *12*, 1104−1113.
(30) Born, M. and Wolf, E. *Principles of Optics*; Pergamon: New York, 1980.
(31) Bellessa, J.; Bonnand, C.; Plenet, J. C.; Mugnier, J. Strong coupling between surface plasmons and excitons in an organic semiconductor. *Phys. Rev. Lett.* **2004**, *93*, 036404.
(32) Schwartz, T.; Hutchison, J. A.; Genet, C.; Ebbesen, T. W. Reversible switching of ultrastrong light-molecule coupling. *Phys. Rev. Lett.* **2011**, *106*, 196405.
(33) *WVASE software package*; J.A. Woollam Co., Inc.: Lincoln, Nebraska, 2014. The measured optical constants of PMMA, Au, and Si are each included as a sum of oscillators in the material library of the software.
(34) Dupertuis, M. A.; Proctor, M.; Acklin, B. Generalization of complex Snell-Descartes and Fresnel laws. *J. Opt. Soc. A* **1994**, *11*, 1159−1166.
(35) Chang, P. C. Y.; Walker, J. G.; Hopcraft, K. I. Ray tracing in absorbing media. *Quant. J. Spectr. Rad. Transfer* **2005**, *96*, 327−341.
(36) Wertheim, G. K.; Butler, M. A.; West, K. W.; Buchanan, D. N. Determination of Gaussian and Lorentzian content of experimental line-shapes. *Rev. Sci. Instrum.* **1974**, *45*, 1369−1371.
(37) Pollard, B.; Muller, E. A.; Hinrichs, K.; Raschke, M. B. Vibrational nano-spectroscopic imaging correlating structure with intermolecular coupling and dynamics. *Nat. Commun.* **2014**, *5*, 1−7.
(38) Wooten, F. *The Optical Properties of Solids*; Academic Press: New York, 1972.
(39) Faucheaux, J. A.; Fu, J.; Jain, P. K. Unified theoretical framework for the realizing diverse regimes of strong coupling between plasmons and electronic transitions. *J. Phys. Chem. C* **2014**, *118*, 2710−2717.